Extreme Mechanics Letters 61 (2023) 102021

Contents lists available at ScienceDirect

Extreme Mechanics Letters

journal homepage: www.elsevier.com/locate/eml

Fast stress wave attenuation in bioinspired composites with distributed soft particles modulating hard matrices

Yingyang Yu [a], Hao Li [a], Xunxun Hu [c], Kun Geng [a], Qiang Zhang [a], Wei Peng [d], Yanan Yuan [a,f], Zuoqi Zhang [a,f,*], Bin Wang [b,e,**]

[a] Department of Engineering Mechanics, School of Civil Engineering, Wuhan University, Wuhan, 430072, PR China
[b] Shenzhen Institute of Advanced Technology, Chinese Academy of Sciences, Shenzhen 518055, PR China
[c] Hubei Institute of Water Resources Survey and Design, Wuhan 430070, PR China
[d] General Design Institute of Hubei Aerospace Technology Academy, Wuhan 430040, PR China
[e] City University of Hong Kong, Hong Kong Special Administrative Region of China
[f] Engineering Research Center on Building Examination and Reinforcement Technology (Ministry of Education), Wuhan University, Wuhan, 430071, PR China

ARTICLE INFO

Article history:
Received 19 January 2023
Received in revised form 14 March 2023
Accepted 12 April 2023
Available online 20 April 2023

Keywords:
Particulate composites
Impact loading
Stress wave
Damping properties
Biomimetic design

ABSTRACT

Fast stress wave attenuation in composites is highly desired in many industry fields. Biological composites such as those in the beak of woodpeckers provide great inspiration for us to develop their synthetic counterparts with similar mechanical functions. Accordingly, bioinspired designs of composites with distributed soft particles are put forward in the paper, and their performance in attenuating stress wave is investigated through FEM simulations. Subjected to projectile impacts, the bioinspired composites not only absorb more impact energy but also delay and attenuate the impact-induced stress wave very efficiently. The simultaneous improvement of the two aspects of impact-resistant performance in a single material design should be highly desired in many industry fields. Further, the influences of the inclusion volume fraction, impedance, shape and distribution pattern are systematically investigated and general principles of design are drawn. The findings and conclusions can not only provide useful guidelines for the design of bioinspired composites with high protection function from impact loading but also help understand the working mechanisms of natural biological composites to resist impact loadings.

1. Introduction

Composites and structures with high performance to resist impact loads and attenuate impact waves are always highly desired in many fields such as military, aerospace, ship, and vehicle industries. Subjected to impact loadings and blast waves, these composites and structures are expected to efficiently block projectiles and attenuate stress waves by absorbing, scattering and dissipating large amounts of energy so that the damage to people and objects behind them can be minimized or eliminated [1]. Load-bearing biological materials and structures such as skull, shell and beak of woodpeckers have been evolved out through long-time and rigorous natural selection and acquired excellent protecting function against dynamic loadings from predators and daily activities [2–6]. Therefore, learning from the material and structural design and relevant working mechanisms of the load-bearing biological materials is definitely helpful for us to develop synthetic materials and structures with high performances of protection functions.

There are many mechanisms working in the stress wave attenuation in composites, generally including stress wave spreading, scattering, energy absorption and dissipation due to the presence of inclusions, interfaces and their resulted deformation and damage behaviors. In engineering, laminated composites are widely used and hence many research efforts have been made to study the stress wave propagation and attenuation in lamellar composites, in which reinforcement materials and matrix materials are usually stacked layer by layer in an alternating way. Due to the elastic impedance mismatch between the layers, as a stress wave reaches the interface between the two materials, only a part of it, i.e., a transmitted wave goes through the interface and continues going forward while the other part, namely a reflected wave is reflected and transmitted backward. Amounts of the reverberations together make dispersive effects and consequently affect

* Corresponding author at: Department of Engineering Mechanics, School of Civil Engineering, Wuhan University, Wuhan, 430072, PR China.
** Corresponding author at: City University of Hong Kong, Hong Kong Special Administrative Region of China.
E-mail addresses: zhang_zuoqi@whu.edu.cn (Z. Zhang), bwang55@cityu.edu.hk (B. Wang).

https://doi.org/10.1016/j.eml.2023.102021
2352-4316/

steady and transient wave shapes, velocities, and attenuation in way analogous to viscosity effects. Barker [7] established a theoretical model for stress wave propagation in lamellar composites by direct analogy with a viscosity effect. Anfinsen [8] studied on the optimum design of layered elastic stress wave attenuators, and determined the optimal materials requirements for the first transmitted stress wave in one-dimensional elastic layered structures. The optimized selection of materials was reported to reduce the stress amplitude more than 99%. Nemat-Nasser et al. [9] designed a layered metamaterial with high attenuation coefficient and high specific in-plane stiffness through minimizing the frequency range of the first pass band, maximizing the frequency range of the stop band, and creating local resonance over the second pass band. With the method of characteristics, Velo and Gazonas [10] obtained explicit formulae of stress in a two-layer elastic strip subjected to transient loading and so identified the optimal designs giving the smallest stress amplitude. Instead of the sharp interfaces within laminate composites, functionally graded materials (FGMs) joining dissimilar materials have attracted a great deal of attention in impact-resistant applications such as armor plating because of their superiority to resist interfacial failure. Bruck [11] proposed a one-dimensional model for designing functionally graded materials to manage stress waves and found that the major benefit of the FGMs over the sharp interface lies in a time delay to the peak reflected stress. With a similar model, Samadhiya et al. [12] studied the time delay and attenuation of the peak reflected stress in FGMs, and demonstrated that the peak stress magnitude attenuates very fast in FGM structures as compared to the sharp interface structure while the time of peak stress arrival is also significantly delayed. Hui and Dutta [13] developed a concept design of ballast and penetration resistant materials with a continuous gradient of impedance so that they can dissipate the shock energy well without common interfacial delamination failure.

Instead of the continuously layered composites intensively studied in engineering fields as aforementioned, many impact-resistant biological composites contain discontinuously fibrous or particulate inclusions. From mechanics perspective, the continuous layer design has some advantages in reflecting and blocking impact waves, but its disadvantages in stiffness and strength are also evident due to the existence of weak and soft layers [14], which may explain why the discontinuous fibrous/particulate and staggered design rather than the continuous layered design is widely adopted in load-bearing biological materials in nature. A famous example of this kind of biological composites is beaks of woodpeckers, which repeatedly strike tree trunks at a high speed up to 7 m/s but show no damage to themselves or brains behind of them [15]. The multi-scale structural characteristics of the beak of red-bellied woodpecker are shown in Fig. 1a, in which the beak at macroscale comprises three structural layers, namely, the outer rhamphotheca layer, the middle foam layer and the inner bony layer. The area fraction of each layer varies along the peak length, analogous to the functionally graded materials. At microscale, the rhamphotheca has keratin scales packed in a staggering pattern, the foam layer is a porous material with distributed voids of different sizes, and the bony layer composed of bundles of collagen fibers has a big center cavity and several small cavities around the one. A number of studies have showed that the cranial bone and beak of woodpecker play crucial roles in impact resistance and energy dissipation [16–21]. For instance, Wang et al. found that the spongy bone as well as its microstructure characteristics such as porosity, trabecular number and thickness are unevenly distributed in the woodpecker's skull, and the uneven distribution feature suits well the protection function of skull to resist impact injury [20]. The microstructures involved in the beak and skull of woodpeckers have inspired material scientists and engineers to develop novel designs of synthetic composites with superior protective functions against dynamic loadings [22–25]. For example, Yoon et al. developed a woodpecker-inspired shock isolator with a microgranular bed to protect micromechanical electronic devices against high-g and high-frequency mechanical excitations [24,25]. Qwamizadeh et al. conducted a series of studies on the stress wave attenuation of the staggering microstructures widely seen in load-bearing biological materials including woodpecker's beak and bone, and proposed the bioinspired staggered composite designs in which short fiber or platelet reinforcements are aligned in a staggered pattern in a matrix [26–29]. They found that the staggered microstructure design can generally provide faster stress decay than the layered design commonly utilized in engineering and there exists an optimal microstructure design (staggered pattern and reinforcement aspect ratio) for given constituent materials and their volume fractions. However, it is noteworthy that all these studies mainly focus on composites with hard reinforcements or inclusions in relatively soft matrices, it is still unclear what will happen for composites with soft reinforcements or inclusions in relatively hard matrices. Moreover, there still lacks of systematic studies on the effects of inclusion shape and distribution pattern on the stress wave attenuation of these bioinspired composites. To this end, the current work carried out studies on the stress wave propagation and attenuation in the bioinspired composites with distributed soft inclusions modulating hard matrices, and a variety of inclusion shapes and distribution patterns are systematically investigated in order to find out the optimal design for fastest stress wave attenuation.

Considering the complexity of the inclusion shapes and distribution patterns, it is a great challenge to obtain a universal analytical solution to well characterize the stress wave propagation and attenuation in the bioinspired composites. Even though some forms of analytical solutions are possible based on homogenization approach, they are difficult to well capture the detailed mechanical behaviors such as stress wave reflection and scattering at the inclusion–matrix interfaces, especially taking the discontinuities and singularities into consideration. Therefore, the numerical simulations via the finite element method (FEM) are adopted to comparatively investigate the stress wave propagation and attenuation of the bioinspired composites subjected to impact loadings. The remaining part of the paper is organized in the following way: the computation setup including FEM model, measure of stress wave attenuation and validation test is described in Section 2, while the results and discussions on the effect of inclusion existence, volume fraction, elastic impedance, shape and distribution pattern are conducted in Section 3; finally, the major findings and conclusions are drawn in Section 4.

2. Computation setup

2.1. FEM model

Two-dimensional plane-strain computational model is utilized here for our studies, and an example of the model is schematically illustrated in Fig. 1b, in which the bioinspired composite with well patterned soft particulate inclusions in relatively hard matrix constitutes an attenuator layer of stress wave, and the attenuator layer is sandwiched by the top and bottom layers of pure hard matrix. Note that the top and bottom layers of pure matrix are designed in purpose to guarantee the same boundary conditions for different designs of the bioinspired composites so that the results and performance are comparable among them. L and H denote the width and height of the model, respectively, along the direction of x and y coordinate, as shown in Fig. 1b. The three layers evenly occupy 1/3 of total height. A flying projectile of plate with dimension h^*L impacts the top boundary of the model

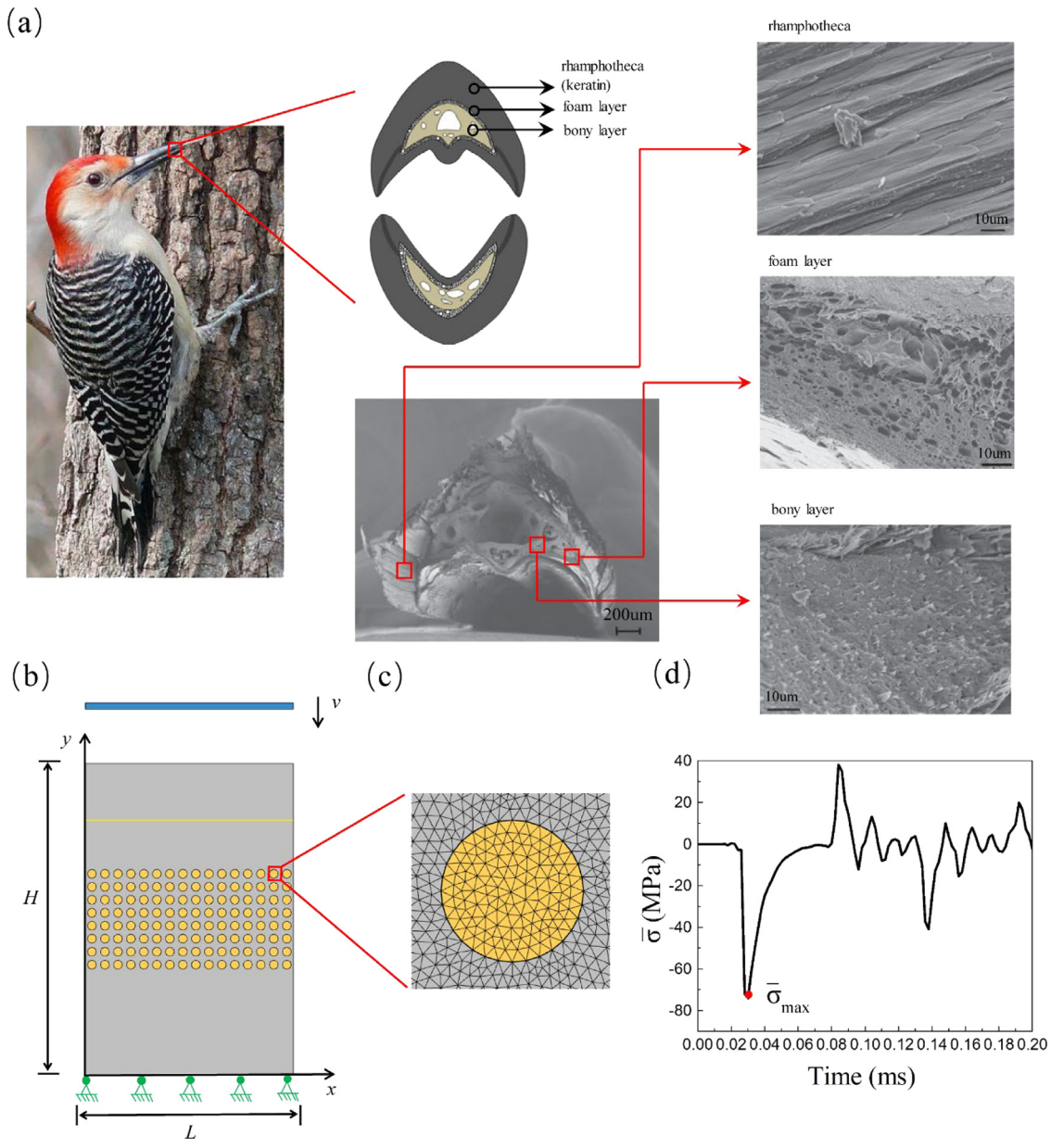

Fig. 1. (a) The hierarchical structural features of the woodpecker's beak, in which particularly staggered arrangement, gradient pattern, and hybrid-sized soft particulate cells/porosities can be seen at microscale; (b) an example of bioinspired composites with soft particles orderly distributed in a relatively harder matrix, the computational setup for simulating the impact wave propagation and attenuation in the bioinspired composites with the finite element method; (c) demonstrates the mesh around a particle; (d) shows a typical time history curve of stress at 96 mm depth (here corresponding to the yellow line in b).. (For interpretation of the references to color in this figure legend, the reader is referred to the web version of this article.)

at an initial velocity v in the y direction. The bottom boundary is fixed, and periodic boundary conditions are prescribed to the left and right edges. The FEM simulations were carried out via one of the popular commercial software COMSOL Multiphysics. A free triangular mesh with the element was adopted for the whole model, see Fig. 1c showing a small part of the mesh for example. In the model, the particles and matrix are perfectly bonded at their interface through sharing nodes. The interface simplification is adopted just in order to focus our current study on the effect of particle distribution pattern, even though it is well known that the interface/interphase always plays a crucial role in the composites' mechanical behaviors [30–32]. The geometrical parameters L=384 mm, H=576 mm and h=12 mm are adopted in our simulations unless otherwise stated. The initial impact velocity of the projectile is set to be a constant v =10 m/s. In the typical example, the circular shape and regularly aligned distribution of inclusions are considered, with a diameter D=16 mm and inter-inclusion spacing d=8 mm here.

As aforementioned, the impact projectile is set to be rigid, and has a density 7850 kg/m^3 similar to that of iron. The materials for soft inclusions and hard matrix were respectively assumed to be silicone rubber and mortar because of their wide applications in many protective buildings and equipment, and to exclusively study the effects of inclusion shape and distribution both of the constituent materials are modeled as linear elastic, with their mechanical properties listed in Table 1. Here, E, ρ, ν, c, and z respectively denote the Young's modulus, density, Poisson's ratio, wave velocity, and elastic impedance. The following relations exist among these material parameters and Lame's constants λ

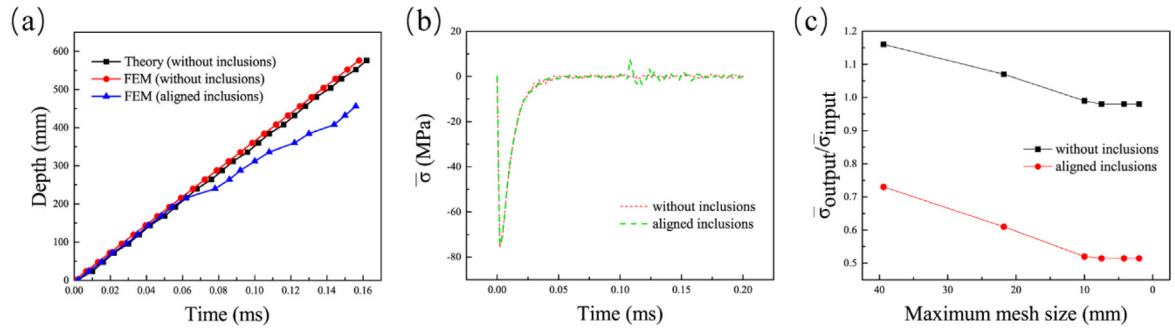

Fig. 2. (a) The impact wave propagation over time in the composites with/without soft inclusions, with the theoretical prediction on the no-inclusion composite included for comparison purpose; (b) the impact stress $\overline{\sigma}$ at the top surface varying with time, almost the same plots seen for the composites with and without soft inclusions before wave reflections come into effect; (c) mesh convergence test by checking the output-to-input stress ratio.

Table 1
Materials and their parameters used in the simulations.

Materials	E/GPa	ρ/kg/m^3	ν	c/m/s	z/kg/m^2/s
Mortar [33]	30	2500	0.2	3650	9.123×10^6
Silicone rubber [30]	3.3×10^{-3}	1245	0.477	143	1.78×10^5

and μ.

$$c = \sqrt{\frac{\lambda + 2\mu}{\rho}} \tag{1}$$

$$\lambda = \frac{\nu E}{(1+\nu)(1-2\nu)} \tag{2}$$

$$\mu = \frac{E}{2(1+\nu)} \tag{3}$$

$$z = \rho c \tag{4}$$

2.2. Measurement of stress wave attenuation

For each element i, we can output its stress at every instant $\sigma_i(t)$ and its area S_i. For a specific depth y=*constant* (e.g., the yellow line in Fig. 1b), we can calculate the average stress at every instant by the following formula:

$$\overline{\sigma} = \sum_{i=1}^{N} \frac{\sigma_i(t) S_i}{S} \tag{5}$$

where the summation is done over all the elements that are crossed by the line y=*constant*. Fig. 1c just shows a typical time history curve of the average stress at y=96 mm. One can see that the impact yielded compressive stress wave reaches the line around 0.024 ms, and the average stress at the line rises quickly to its maximum value around 0.03 ms. Then, the average stress gradually reduces to zero as the incident stress wave leaves the line behind. When part of the incident stress wave is reflected by the distributed inclusions and comes back to the line, the average stress reverses to tension and reaches a tension peak quickly. As the stress waves reverberate again and again, the average stress at the line oscillates up and down; however, the peak values are always decreasing over time. It is noteworthy that the effect of the stress wave reflection at the bottom boundary is excluded for simplicity purposes. Denote the maximum magnitude of the average stress as $\overline{\sigma}_{max}$, and then the change of $\overline{\sigma}_{max}$ over depth can be obtained to quantitatively characterize the stress attenuation.

Define the input magnitude of the stress wave $\overline{\sigma}_{input} = \overline{\sigma}_{max}$ in the top layer of pure matrix (e.g., y=96 mm) before the impact stress wave enters the bioinspired composite layer, while the output magnitude of the stress wave $\overline{\sigma}_{output} = \overline{\sigma}_{max}$ in the bottom layer of pure matrix (e.g., y=480 mm) after the impact stress wave goes through the bioinspired composite layer. Then, the stress wave attenuation rate can be defined according to the following formula

$$R_F = 1 - \frac{\overline{\sigma}_{output}}{\overline{\sigma}_{input}} \tag{6}$$

2.3. Mesh convergence and validation test

As aforementioned, the analytical solution of the wave propagation characteristics in the bioinspired composites is not available, and hence our computational model was first applied to the pure matrix material (without inclusions) for validation purpose. For the pure matrix material case, the reliable theoretical solution is available. As shown in Fig. 2a, our computational results of the stress wave propagating depth over time agree well with the theoretical solution, suggesting the reliability of our computational model. Fig. 2b plots the time–history curves of impact stress at the top surface for the models with and without soft inclusions. One can see that the two curves coincide with each other before the inclusion-induced reflection waves come back (the time about 0.105 ms), and so the impact-loading boundary condition and resulted incident stress wave are well guaranteed to be consistent for different designs of the bioinspired composite in the middle layer. In particular, the amplitude and duration of the transient load from the impact of the rigid projectile can also be obtained, respectively, 75.4 MPa and 0.04 ms. The impulse width can be estimated to be $l = ct = 146$ mm, much less than the structure width H=576 mm, satisfying the requirement suggested by the Ref. [34]. For a good balance between the computational efficiency and accuracy, the element size l_e ($l_e \leq \frac{l}{20}$) should be no larger than 7.3 mm and the time increment Δt ($\frac{1}{\sqrt{2}}\frac{l_e}{c} \leq \Delta t \leq \frac{l_e}{c}$) should be in the range of $1.4 \times 10^{-6} \sim 2 \times 10^{-6}$ s. Fig. 2c suggests that the output-to-input stress ratios gradually converge with the decrease of the maximum element size, and the element size $l_e = 7.3$ mm is sufficient to provide convergent and reliable computational results in our simulations.

3. Results and discussion

3.1. Comparison between the composites with and without soft inclusions

In order to show the effects of soft inclusions, the stress wave propagation and attenuation were compared between the model (see Fig. 1b) with and without the soft inclusions. Fig. 3a presents the projectile velocity varying with time. One can see that the two curves are almost the same except that the rebounding time is delayed and the rebounding velocity is reduced for the model

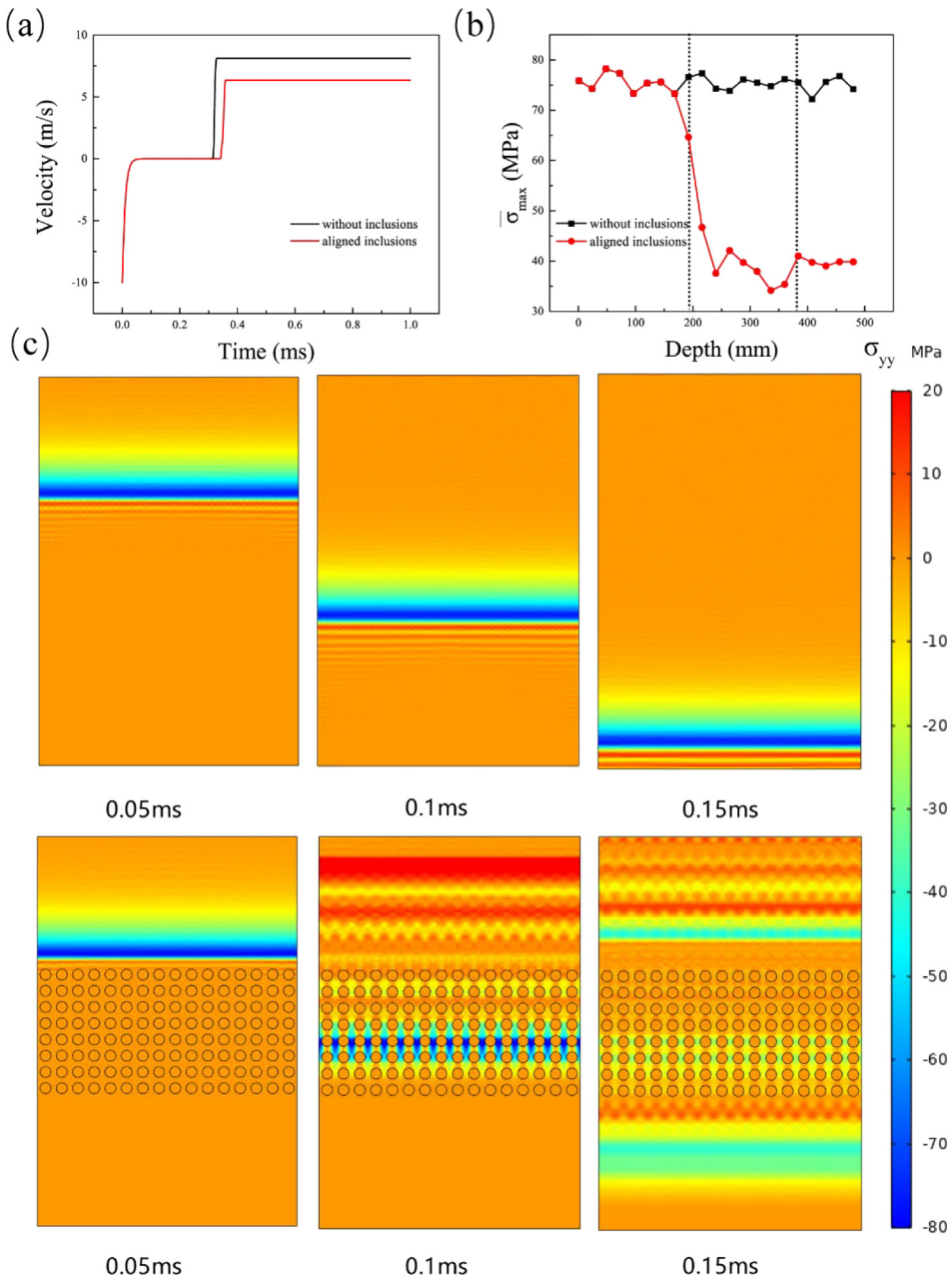

Fig. 3. (a) The time history plots of the projectile velocity during the impact; (b) the stress wave attenuation along the depth the stress wave going down; (c) the stress contour snapshots as the impact stress wave propagating in the composite without soft inclusions, and the composite with regularly distributed soft inclusions.

with soft inclusions. This indicates that the system with the soft inclusions absorbs more impact energy. The difference is easily understood because of the softening effect of the soft inclusions to the composite structure. Fig. 3b shows the plots of the maximum average stress changing with the propagation depth for the two systems. It can be found that in the top layer of pure matrix, the stress magnitudes for the two systems are the same, but there is about 50% attenuation after the stress wave going through the middle layer of bioinspired composite while no attenuation at all in the pure matrix system. The underlying mechanism is evident if we check the snapshots of stress contour of the two systems (see Fig. 3c). The stress contours at different instant of time clearly show that in the model without soft inclusions, the stress wave propagates in a steady state without attenuation in the homogeneous and elastic media just as expected, whereas in the model with the bioinspired layer of aligned soft inclusions the stress wave is scattered and reflected by these inclusions so that the arrival of the peak stress is distinctly delayed and the magnitude of the peak stress is significantly reduced.

3.2. Effect of the inclusions volume fraction

From the perspective of composite design, volume fraction is certainly one of the primary factors to be considered. Here the soft inclusion volume fraction is altered by changing the inclusion diameter D and correspondingly the inter-inclusion spacing d, and its influences of on the projectile rebounding velocity, stress–depth curve and stress wave attenuation are shown in Fig. 4a-c, respectively. We can see that the projectile rebounding velocity is always decreasing with increasing the volume fraction of soft inclusions, indicating that the part of energy absorbed by the composite system is increasing. It is in line with the classic impact theory that the softer is the target plate of composite, the more is the energy absorbed by the target plate and correspondingly the

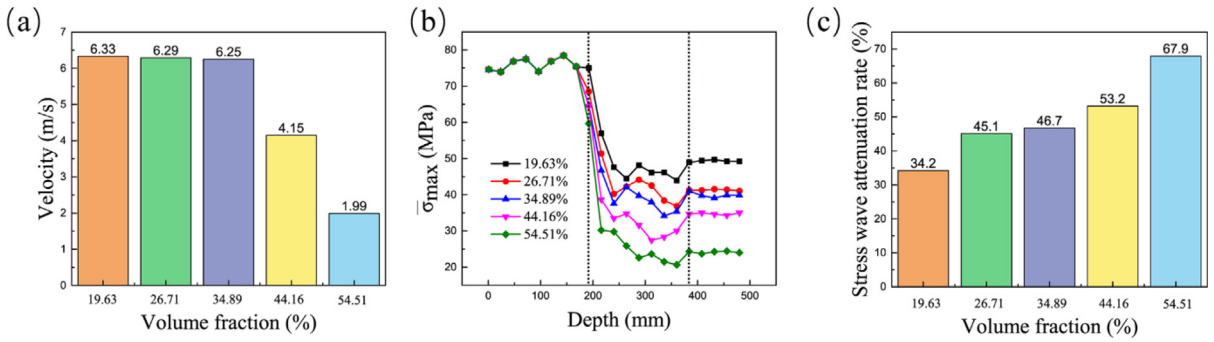

Fig. 4. Comparisons of the projectile rebounding velocity (a), stress–depth curve (b) and stress wave attenuation rate (c) among the bioinspired composites with different volume fraction of soft inclusions.

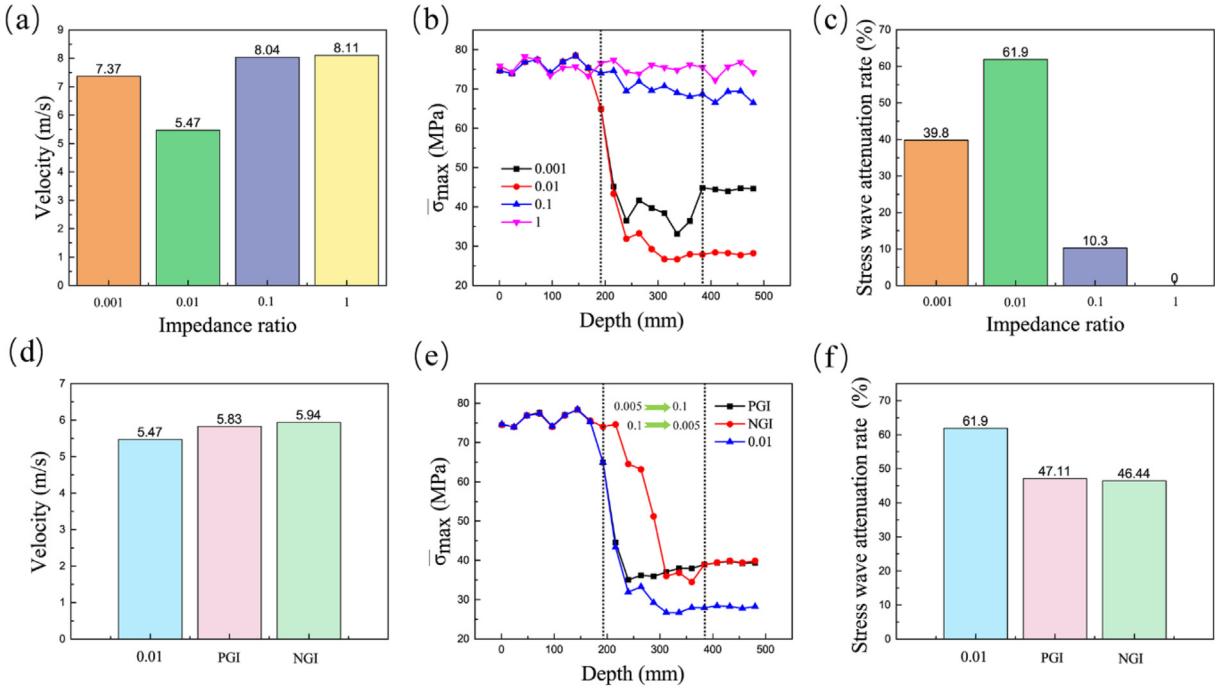

Fig. 5. Comparisons of the projectile rebounding velocity (a), stress–depth curve (b) and stress wave attenuation rate (c) among the bioinspired composites with different inclusion–matrix impedance ratios; the impedance gradient effect on the projectile rebounding velocity (d), stress–depth curve (e) and stress wave attenuation rate (f).

less is the energy rebounded. Fig. 4b shows that through the layer of bioinspired composite the magnitude of peak stress goes down faster and to a lower level as the soft inclusion volume fraction goes higher. Consequently, the stress wave attenuation rate also increases with the volume fraction of soft inclusions, as shown in Fig. 4c. The trends are reasonable, since the inclusion diameter increases and their spacing decreases with the volume fraction increasing so that the stress wave scattering and reverberating among the inclusions are elevated and the blocking and delaying effects are enhanced.

It is worth noting that the bioinspired composites with distributed soft inclusions modulating hard matrices not only absorb more impact energy but also attenuate the impact-induced stress wave more efficiently, the simultaneous achievement of which two aspects of the impact-resistant performance in a single material design is highly desired in many industry fields. The computational results here suggest that the impact-resistant performance of the bioinspired composites seems continuously improved with the soft inclusion volume fraction increasing up to more than 50%. However, we should keep in mind that a very large volume fraction of soft inclusions would inevitably sacrifice the effective stiffness and strength of composites, and an elegant balance between dynamic and static performance is necessary for material design in most industry areas.

3.3. Effect of the inclusion–matrix impedance ratio

Here both of the constituent materials are linear elastic, and hence the stress wave attenuation is mainly resulted from the stress wave reflection at the inclusion–matrix interface due to their elastic impedance mismatch. In this section, the influence of the inclusion–matrix impedance ratio on the impact-resistant behaviors is investigated in order to get some principal guidelines for the constituent material selection. The results are shown in Figs. 5a-c, respectively, as the rebounding velocity of projectile, the stress–depth curve and stress wave attenuation rate varying with respect to the inclusion–matrix impedance ratio. One can see that the performance of composites does not change monotonically with the varying of the impedance ratio. Generally, relatively large impedance mismatch (e.g., the impedance ratio equal to 0.01 and 0.001) between the inclusion and matrix is necessary to gain significant stress wave attenuation. As the impedance

ratio increases from 0.001 to 0.01, 0.1 and 1, the rebounding velocity of projectile first decreases and then increases. The bioinspired composite design with the inclusion–matrix impedance ratio of 0.01 gives the smallest rebounding velocity and correspondingly provides the best capability of impact energy absorption. The stress wave attenuation rate first increases and then decreases with the increase of the impedance ratio. The largest stress wave attenuation is achieved with the bioinspired composite design with the inclusion–matrix impedance ratio of 0.01 too. In the bioinspired composites with distributed soft inclusions modulating hard matrices, the impact energy absorbing capacity and the stress wave attenuation capability seem synchronized and can be simultaneously optimized with one single design. This is a great advantage for potential applications of the bioinspired composites in many industry fields. The optimal inclusion–matrix impedance ratio exists for maximum stress wave attenuation, probably because proper selections of the inclusion material make one of the natural frequencies of the composite close to the frequency of the impact-yielded stress wave and so the damping mechanism of local resonance would be excited. To verify this argument, we calculated the first-order inherent frequency of the unit cell of different impedance ratio, and the results show that the unit cells of different impedance ratio own different inherent frequency (see Fig. S1a in the supplementary material). Further, we took the composite with inclusion–matrix impedance ratio of 0.01 for an example, and applied an incident sine stress wave with varying frequency. The plot of the stress wave attenuation rate versus the incident stress wave frequency clearly shows that the stress wave attenuation rate reaches its maximum value when the frequency of incident stress wave is around the inherent frequency (see Fig. S1b in the supplementary material). The similar phenomenon and working mechanism have also been reported in the literature [35,36].

In addition to the scenario of single inclusion material considered above, we also probed the effect of impedance gradient in inclusions. Specifically, there are two types of impedance gradient with inclusion materials investigated: the positive gradient of impedance (PGI), i.e., inclusion elastic impedance increasing from top down (here the inclusion–matrix impedance ratio from 0.005, 0.01, 0.05, to 0.1 as an example), and the negative gradient of impedance (NGI), i.e., inclusion elastic impedance decreasing from top down (here the inclusion–matrix impedance ratio from 0.1, 0.05, 0.01, to 0.005 as an example). The results of projectile rebounding velocity, stress–depth curve and stress wave attenuation rate are respectively shown in Figs. 5d-f, alongside of the constant impedance case (here the inclusion–matrix impedance ratio 0.01 adopted) for comparison purposes. We can see that the gradient of impedance in inclusions only leads to a slight increase in the projectile rebounding velocity but a significant decrease in the stress wave attenuation. PGI and NGI yield similar results in the projectile rebounding velocity and stress wave attenuation rate, but the onset of distinct jump in the stress–depth curve for NGI is delayed a little (see Fig. 5e) due to the small inclusion–matrix impedance mismatch around its top edge.

3.4. Effect of the shape of soft inclusions

The local stress wave scattering is highly dependent on the inclusion shape, and hence the effect of inclusion shape is studied in this section. As illustrated by the insets in Fig. 6a, two types of inclusion shape are considered: one is ellipse and the other is rectangle. The former is smooth while the latter is with corners. Their horizontal (x direction, perpendicular to the impact direction) and vertical (y direction, parallel to the impact direction) dimensions are respectively denoted as a and b, and the dimension ratio α is defined by $\alpha = a/b$. Fix the volume fraction of inclusions, vary the dimension ratio, and the bioinspired composites with different shapes of soft inclusions can be obtained for the comparative studies. Here the volume fraction of soft inclusions is set to be 34.89%, and three dimension ratios of 0.64, 1 and 1.5625 are taken as representative examples of the three scenarios: the shorter axis/edge perpendicular to the impact direction, the circular/square shape, and the longer axis/edge perpendicular to the impact direction in sequence. Their impact-resistant performances are compared in Fig. 6. First of all, the ellipse and rectangle shapes with the same dimension ratio only yield marginal differences in the projectile rebounding velocity, stress–depth curve as well as the stress wave attenuation rate. This indicates that the stress wave propagation and attenuation in the bioinspired composites seems not sensitive to the existence of corners on the soft inclusions. As the dimension ratio increases, the rebounding velocity of projectile always decreases and the stress wave attenuation rate always increases for both the ellipse and rectangle inclusions. It can be inferred that, the larger is the inclusion dimension facing to the stress wave propagation direction, the more is the impact energy absorbed, and the faster is the stress wave attenuation. These results can be further evidenced by their snapshots of stress contours at the instant $t = 0.15$ ms. We can see that the bioinspired composites with larger α distinctly elongate the penetration time and reduce the magnitude of stress waves. From another perspective, the studies here actually demonstrate the anisotropic characteristics of the bioinspired composites, and they exhibit superior impact-resistant performance in the transverse direction (corresponding to the example $\alpha = 1.5625$ here) over the longitudinal direction (corresponding to the example $\alpha = 0.64$ here). Regarding the static stiffness and strength, the longitudinal direction is usually superior to the transverse direction, that is so-called longitudinal superiority featuring in many load-bearing biological materials such as bones [37,38]. Combination of these findings brings us a novel insight into the biological design of composites like bones, i.e., the longitudinal direction owning higher stiffness and strength well suits to bear the static physiological loadings such as body weights while the transverse direction having higher impact-resistant properties well fits to protect the fragile organs such as bone marrow from impact loadings.

3.5. Effect of the distribution pattern of soft inclusions

As mentioned in the introduction section, the staggered, gradient and hybrid distributions of reinforcements are widely seen in load-bearing biological composites due to their respective advantages. Interesting questions arises: Compared to the aligned distribution pattern, are the staggered, gradient and hybrid distribution patterns better in the impact-resistant performances? Further, which one is the best among them? To answer these questions, a variety of distribution patterns listed in Fig. 7 are studies for comparison purposes. In the gradient group, there are four variations investigated, namely, the positive gradient (PG, particle increasing from top down), the negative gradient (NG, particle decreasing from top down), the positive–negative gradient (PNG, particle first increasing and then decreasing from top down), and the negative–positive gradient (NPG, particle first decreasing and then increasing from top down). The hybrid distribution involves particulate inclusions of two sizes arranged in an alternating way, and it has four variations, namely, the small–large hybrid (SLH), the large–small hybrid (LSH), the combining staggered and small–large hybrid (SSLH), and the combining staggered and large–small hybrid (SLSH).

The results of projectile rebounding velocity, stress–depth curve and stress wave attenuation rate were respectively shown in Figs. 8a-c for all the distribution patterns in Fig. 7, with the

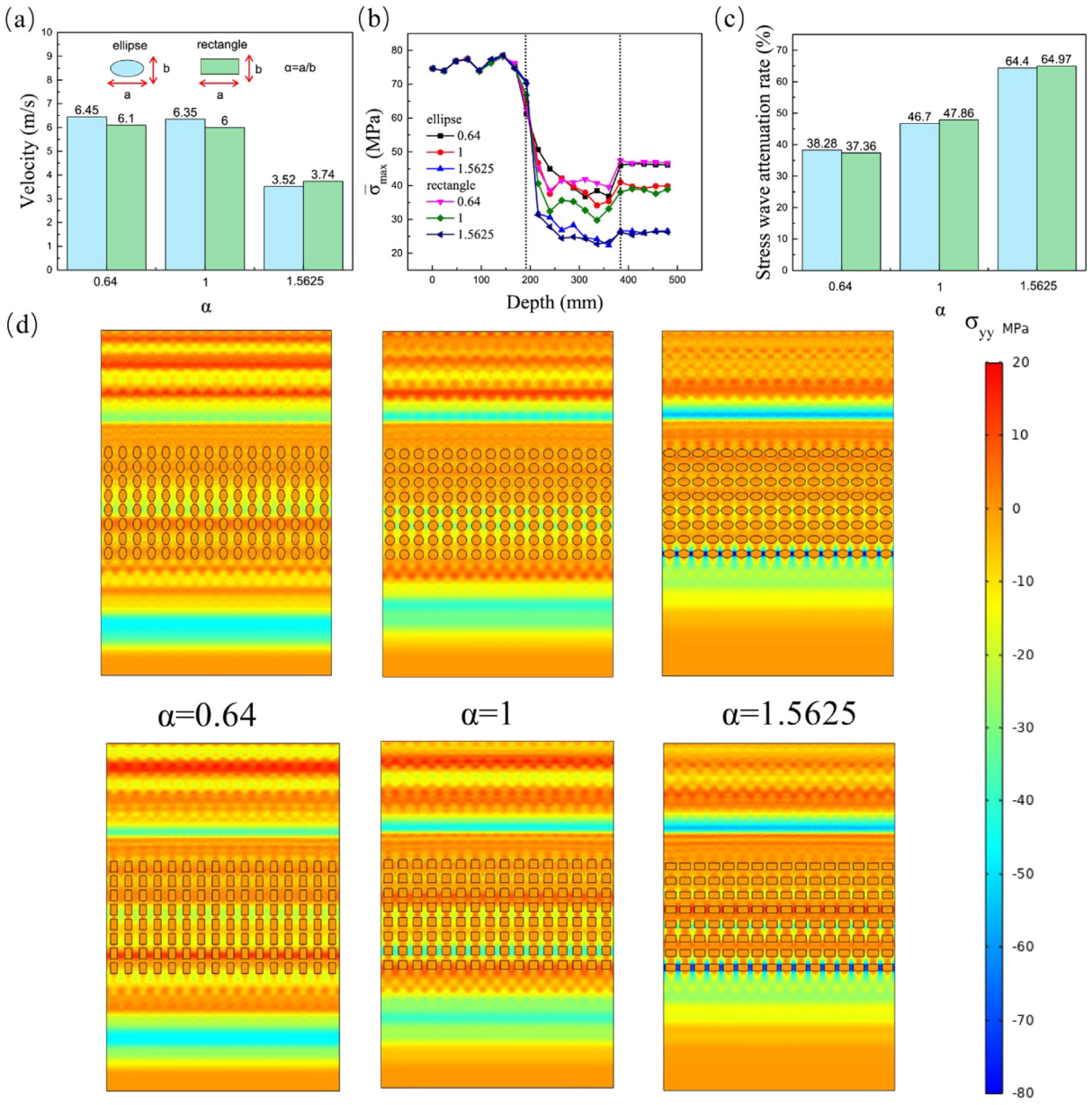

Fig. 6. Comparisons of the projectile rebounding velocity (a), stress–depth curve (b) and stress wave attenuation rate (c) among the bioinspired composites with different shapes of soft-inclusions; (d) show the snapshots of their stress contours at the instant $t = 0.15$ ms.

pure matrix material without any inclusions included as a base reference. Noteworthy that the volume fraction of soft inclusions are kept to be the same, 34.89% for all the composites. Generally speaking, the rebounding velocity of projectile decreases from the aligned distribution to the staggered distribution, the gradient distribution and the hybrid distribution, in sequence. Specifically, within the group of gradient distribution the descending order in terms of the rebounding velocity is NG>PG>PNG>NPG, whereas within the group of hybrid distribution the order is LSH>SLSH>SLH>SSLH. Note that the NPG distribution yields the least rebounding velocity, while the SSLH distribution gives a slightly larger value. Regarding the stress wave attenuation, the stress wave attenuation rate generally increases from the aligned distribution to the staggered, the gradient and the hybrid. In the group of gradient distribution, the PG, NG and PNG distributions give similar results in the stress wave attenuation rate, but the NPG distribution provides a significantly larger attenuation rate than them. With respect to the hybrid distribution, the SLH just slightly outperforms the LSH. The advantage of the hybrid distribution in stress wave attenuation has also been mentioned by R. Rafiee-Dehkharghani [39]. By comparing SSLH and SLSH with SLH and LSH, respectively, we can see that the introduction of staggered feature into the hybrid distribution patterns further slightly decreases the rebounding velocity of the projectile and increases the stress wave attenuation rate, indicating the positive superimposition effect of the two distribution features. Among all these distributions, the SSLH exhibits the best performance in attenuating stress wave. Fig. 8d shows the snapshots of stress contours at the instant t=0.15 ms for these different distributions of soft inclusions. We can see that, with comparison to the other distribution patterns, the hybrid distribution patterns (SLH, LSH, SSLH and SLSH) filter and spread the incident stress wave into

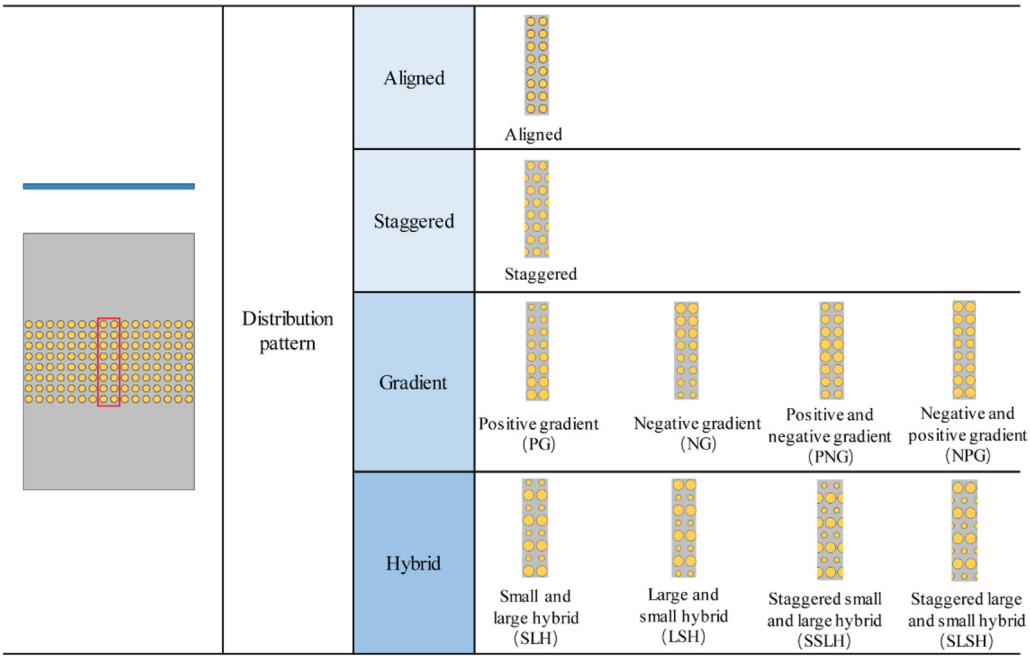

Fig. 7. A list of variations in the distribution pattern of soft inclusions.

multiple stress waves of small magnitude, and they reduce the maximum stress magnitude more significantly. These results and findings generally show us that given the constituent materials and their fraction, and even the inclusion shape, the design of distribution pattern is still an efficient way to tune the composites' mechanical characteristics in stress wave propagation and attenuation. Moreover, the general principle of design can also be drawn here: the staggered pattern is better than the aligned pattern, the gradient pattern better than the uniform pattern, and the hybrid pattern is best. Although the comparative study on several examples of the bioinspired distribution patterns in Fig. 7 is preliminary, the trends unveiled here would be helpful to the microstructure selection and design of composites for high impact-resistant performances.

4. Summary

Fast stress wave attenuation in composites is highly desired in many industry fields. Biological composites such as those in the beak of woodpeckers provide great inspiration for us to develop their synthetic counterparts with similar mechanical functions. With FEM simulations, the current work conducted a systematic study on the stress wave propagation and attenuation in the bioinspired composites with distributed soft inclusions modulating hard matrices, and the effects of inclusion volume fraction, elastic impedance, shape and distribution pattern are systematically investigated. The following major conclusions can be drawn:

1. With comparison to the homogeneous and elastic media, the bioinspired composites with distributed soft inclusions modulating hard matrices not only absorb more impact energy (corresponding to smaller rebounding velocity of impact projectile) but also delay and attenuate the impact-induced stress wave very efficiently. The simultaneous improvement of the two aspects of the impact-resistant performance in a single material design is highly desired in many industry fields.

2. In terms of absorbing impact energy and attenuate stress waves, the impact-resistant performance of the bioinspired composites is shown continuously improved with the soft inclusion volume fraction increasing up to more than 50%. There is an optimal inclusion–matrix impedance ratio for the maximum impact energy absorption and stress wave attenuation, indicating that the impedance mismatch is not the larger, the better.

3. Regarding the influence of the inclusion shape, the ellipse and rectangle exhibit similar stress wave attenuation performance provided that their dimension ratios are the same. However, their performance is better when their larger dimension faces to the propagation direction of impact stress waves. From another perspective, the anisotropic characteristics of the bioinspired composites in impact resistant behaviors are unveiled: they exhibit superior impact-resistant performance in the transverse direction (along the small dimension) over the longitudinal direction (along the large dimension). The transverse superiority of biological designs in protective function against dynamic loadings including impact is well complimentary with their longitudinal superiority [37,38] in supporting function against static loadings such as body weight.

4. The distribution pattern of soft inclusions demonstrates critically important influence on the impact energy absorption and stress wave attenuation behaviors. Among the bioinspired distribution patterns considered in our paper, we found the general principle of design: the staggered pattern is better than the aligned pattern, the gradient pattern better than the uniform pattern, and the hybrid pattern is best.

It is also worth noting that, with the bioinspired composites with distributed soft inclusions modulating hard matrices, the varying of impact energy absorption and stress wave attenuation are generally synchronized over all the influence factors considered here, suggesting that the two properties can be simultaneously optimized with one single design. The findings and conclusions here not only provide useful guidelines for the

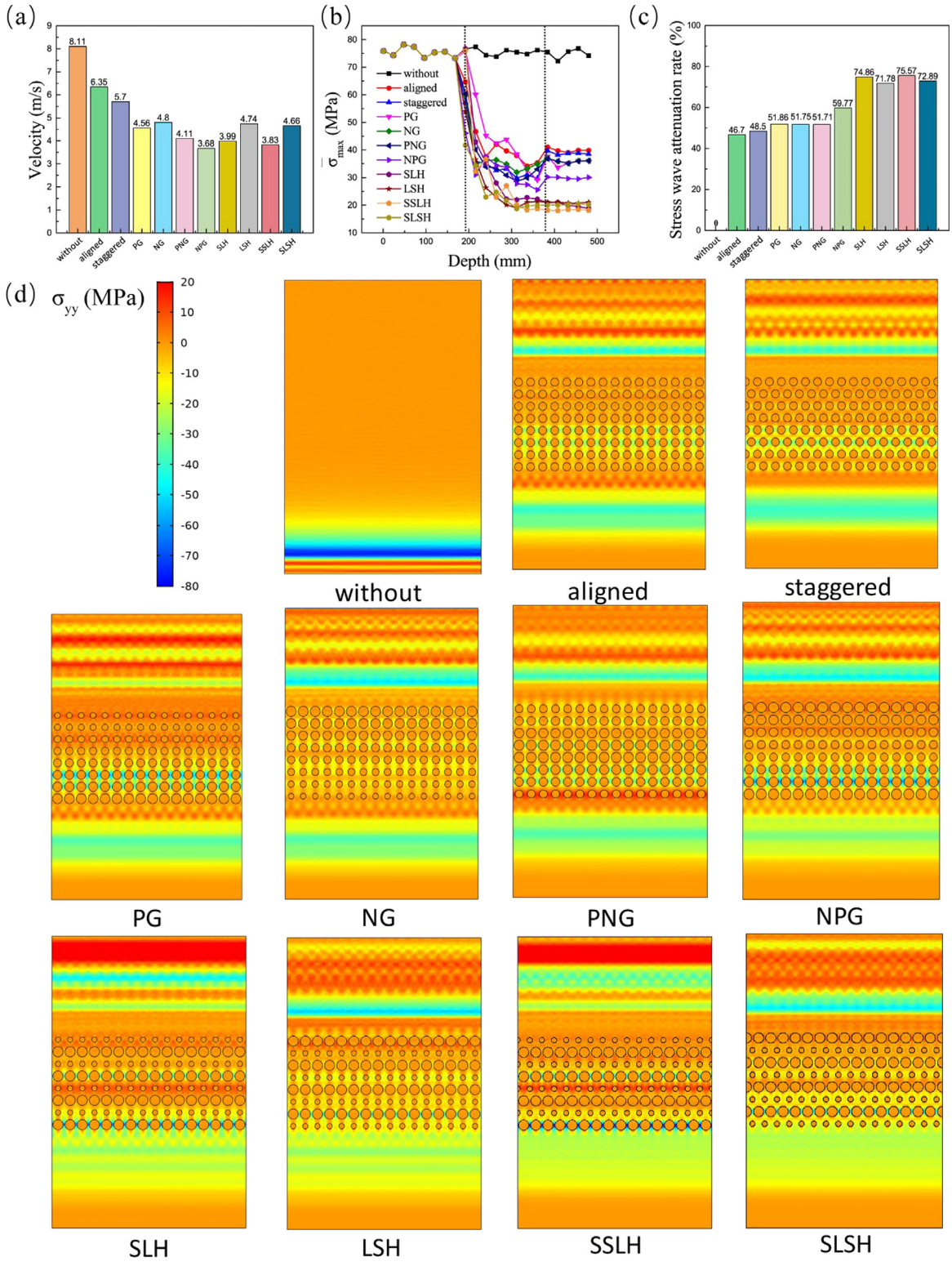

Fig. 8. Comparisons of the projectile rebounding velocity (a), stress–depth curve (b) and stress wave attenuation rate (c) among the bioinspired composites with different distribution patterns of soft-inclusions; (d) show the snapshots of their stress contours at the instant t = 0.15 ms.

design of bioinspired composites with high protection function from impact loading, but also can help understand the working mechanisms of natural biological composites to resist impact loadings. However, the work is still preliminary with some important factors such as inclusion–matrix interface and material viscosity being excluded for simplification purposes, and further studies dedicated to these factors are definitely desired in this research area.

Declaration of competing interest

The authors declare that they have no known competing financial interests or personal relationships that could have appeared to influence the work reported in this paper.

Data availability

No data was used for the research described in the article.

Acknowledgments

The work was supported by National Natural Science Foundation of China (Grant Nos. 11720101002, 11772240, 11542001, 52075528) and Shenzhen-Hong Kong Joint Innovation Project, PR China (No. SGDX2019091716460172).

Appendix A. Supplementary data

Supplementary material related to this article can be found online at https://doi.org/10.1016/j.eml.2023.102021.

References

[1] E.A. Flores-Johnson, L. Shen, I. Guiamatsia, G.D. Nguyen, Numerical investigation of the impact behaviour of bioinspired nacre-like aluminium composite plates, Compos. Sci. Technol. 96 (2014) 13–22, http://dx.doi.org/10.1016/j.compscitech.2014.03.001.

[2] J. McKittrick, P.Y. Chen, L. Tombolato, E.E. Novitskaya, M.W. Trim, G.A. Hirata, et al., Energy absorbent natural materials and bioinspired design strategies: A review, Mater. Sci. Eng. C 30 (3) (2010) 331–342, http://dx.doi.org/10.1016/j.msec.2010.01.011.

[3] J. Huang, H. Durden, M. Chowdhury, Bio-inspired armor protective material systems for ballistic shock mitigation, Mater. Des. 32 (7) (2011) 3702–3710, http://dx.doi.org/10.1016/j.matdes.2011.03.061.

[4] H. Essabir, E. Hilali, A. Elgharad, H. El Minor, A. Imad, A. Elamraoui, et al., Mechanical and thermal properties of bio-composites based on polypropylene reinforced with Nut-shells of Argan particles, Mater. Des. 49 (2013) 442–448, http://dx.doi.org/10.1016/j.matdes.2013.01.025.

[5] P. Liu, D. Zhu, Y. Yao, J. Wang, T.Q. Bui, Numerical simulation of ballistic impact behavior of bio-inspired scale-like protection system, Mater. Des. 99 (2016) 201–210, http://dx.doi.org/10.1016/j.matdes.2016.03.040.

[6] F. Barthelat, Biomimetics for next generation materials, Philos. Trans. A Math. Phys. Eng. Sci. 365 (1861) (2007) 2907–2919, http://dx.doi.org/10.1098/rsta.2007.0006.

[7] L.M. Barker, A model for stress wave propagation in composite materials, J. Compos. Mater. 5 (2) (2016) 140–162, http://dx.doi.org/10.1177/002199837100500202.

[8] L.E. Anfinsen, Optimum design of layered elastic stress wave attenuators, J. Appl. Mech. 34 (3) (1967) 751–755, http://dx.doi.org/10.1115/1.3607771.

[9] S. Nemat-Nasser, H. Sadeghi, A.V. Amirkhizi, A. Srivastava, Phononic layered composites for stress-wave attenuation, Mech. Res. Commun. 68 (2015) 65–69, http://dx.doi.org/10.1016/j.mechrescom.2015.05.001.

[10] A.P. Velo, G.A. Gazonas, Optimal design of a two-layered elastic strip subjected to transient loading, Int. J. Solids Struct. 40 (23) (2003) 6417–6428, http://dx.doi.org/10.1016/s0020-7683(03)00438-4.

[11] H.A. Bruck, A one-dimensional model for designing functionally graded materials to manage stress waves, Int. J. Solids Struct. 37 (44) (2000) 6383–6395, http://dx.doi.org/10.1016/s0020-7683(99)00236-x.

[12] R. Samadhiya, A. Mukherjee, S. Schmauder, Characterization of discretely graded materials using acoustic wave propagation, Comput. Mater. Sci. 37 (1–2) (2006) 20–28, http://dx.doi.org/10.1016/j.commatsci.2005.12.036.

[13] D. Hui, P.K. Dutta, A new concept of shock mitigation by impedance-graded materials, Composites B 42 (8) (2011) 2181–2184, http://dx.doi.org/10.1016/j.compositesb.2011.05.016.

[14] Z.Q. Zhang, B. Liu, Y. Huang, K.C. Hwang, H. Gao, Mechanical properties of unidirectional nanocomposites with non-uniformly or randomly staggered platelet distribution, J. Mech. Phys. Solids 58 (10) (2010) 1646–1660, http://dx.doi.org/10.1016/j.jmps.2010.07.004.

[15] N. Lee, M.F. Horstemeyer, H. Rhee, B. Nabors, J. Liao, L.N. Williams, Hierarchical multiscale structure–property relationships of the red-bellied woodpecker (Melanerpes carolinus) beak, J. R. Soc. Interface 11 (96) (2014) 20140274, http://dx.doi.org/10.1098/rsif.2014.0274.

[16] L. Wang, H. Zhang, Y. Fan, Comparative study of the mechanical properties, micro-structure, and composition of the cranial and beak bones of the great spotted woodpecker and the lark bird, Sci. China Life Sci. 54 (11) (2011) 1036–1041, http://dx.doi.org/10.1007/s11427-011-4242-2.

[17] L.J. Gibson, Woodpecker pecking: how woodpeckers avoid brain injury, J. Zool. 270 (3) (2006) 462–465, http://dx.doi.org/10.1111/j.1469-7998.2006.00166.x.

[18] L. Wang, J.T.-M. Cheung, F. Pu, D. Li, M. Zhang, Y. Fan, Why do woodpeckers resist head impact injury: A biomechanical investigation, PLoS One 6 (10) (2011) e26490, http://dx.doi.org/10.1371/journal.pone.0026490.

[19] Y. Liu, X. Qiu, X. Zhang, T.X. Yu, Response of woodpecker's head during pecking process simulated by material point method, PLoS One 10 (4) (2015) e0122677, http://dx.doi.org/10.1371/journal.pone.0122677.

[20] L. Wang, X. Niu, Y. Ni, P. Xu, X. Liu, S. Lu, et al., Effect of microstructure of spongy bone in different parts of woodpecker's skull on resistance to impact injury, J. Nanomater. 2013 (2013) 924564, http://dx.doi.org/10.1155/2013/924564.

[21] Z.D. Zhu, G.J. Ma, C.W. Wu, Z. Chen, Numerical study of the impact response of woodpecker's head, AIP Adv. 2 (4) (2012) 042173, http://dx.doi.org/10.1063/1.4770305.

[22] J.C. Najmon, D.J. Jacob, Z.M. Wood, A. Tovar, Cellular helmet liner design through bio-inspired structures and topology optimization of compliant mechanism lattices, SAE Int. J. Transp. Saf. 6 (3) (2018) 217–236, http://dx.doi.org/10.4271/2018-01-1057.

[23] J. Ezemba, A. Layton, Bio-inspired avenues for advancing brain injury prevention, J. Mech. Des. 144 (12) (2022) http://dx.doi.org/10.1115/1.4055737.

[24] S.-H. Yoon, S. Park, A mechanical analysis of woodpecker drumming and its application to shock-absorbing systems, Bioinspiration Biomim. 6 (1) (2011) 016003, http://dx.doi.org/10.1088/1748-3182/6/1/016003.

[25] S.-H. Yoon, J.-E. Roh, K.L. Kim, Woodpecker-inspired shock isolation by microgranular bed, J. Phys. D: Appl. Phys. 42 (3) (2009) 035501, http://dx.doi.org/10.1088/0022-3727/42/3/035501.

[26] M. Qwamizadeh, M. Lin, Z. Zhang, K. Zhou, Y.W. Zhang, Bounds for the dynamic modulus of unidirectional composites with bioinspired staggered distributions of platelets, Compos. Struct. 167 (2017) 152–165, http://dx.doi.org/10.1016/j.compstruct.2017.01.077.

[27] M. Qwamizadeh, P. Liu, Z. Zhang, K. Zhou, Y. Wei Zhang, Hierarchical structure enhances and tunes the damping behavior of load-bearing biological materials, J. Appl. Mech. 83 (5) (2016) 051009, http://dx.doi.org/10.1115/1.4032861.

[28] M. Qwamizadeh, Z. Zhang, K. Zhou, Y.W. Zhang, On the relationship between the dynamic behavior and nanoscale staggered structure of the bone, J. Mech. Phys. Solids 78 (2015) 17–31, http://dx.doi.org/10.1016/j.jmps.2015.01.009.

[29] M. Qwamizadeh, Z. Zhang, K. Zhou, Y.W. Zhang. Protein viscosity, Mineral fraction and staggered architecture cooperatively enable the fastest stress wave decay in load-bearing biological materials, J. Mech. Behav. Biomed. Mater. 60 (2016) 339–355, http://dx.doi.org/10.1016/j.jmbbm.2016.02.016.

[30] S.J. Mitchell, A. Pandolfi, M. Ortiz, Metaconcrete: designed aggregates to enhance dynamic performance, J. Mech. Phys. Solids 65 (2014) 69–81, http://dx.doi.org/10.1016/j.jmps.2014.01.003.

[31] Z. Liu, X. Zhang, Y. Mao, Y.Y. Zhu, Z. Yang, C.T. Chan, et al., Locally resonant sonic materials, Science 289 (5485) (2000) 1734–1736, http://dx.doi.org/10.1126/science.289.5485.1734.

[32] Z. Liu, C.T. Chan, P. Sheng, Analytic model of phononic crystals with local resonances, Phys. Rev. B 71 (1) (2005) http://dx.doi.org/10.1103/PhysRevB.71.014103.

[33] G. Ma, C. Fu, G. Wang, P. Del Hougne, J. Christensen, Y. Lai, et al., Polarization bandgaps and fluid-like elasticity in fully solid elastic metamaterials, Nature Commun. 7 (2016) 13536, http://dx.doi.org/10.1038/ncomms13536.

[34] R. Rafiee-Dehkharghani, A.J. Aref, G.F. Dargush, Characterization of multi-layered stress wave attenuators subjected to impulsive transient loadings, J. Eng. Mech. 141 (4) (2015) http://dx.doi.org/10.1061/(asce)em.1943-7889.0000859.

[35] M. Hirsekorn, Small-size sonic crystals with strong attenuation bands in the audible frequency range, Appl. Phys. Lett. 84 (17) (2004) 3364–3366, http://dx.doi.org/10.1063/1.1723688.

[36] D. Xu, Y. Guo, Local resonant attenuation of stress waves in particulate composites, Materials (Basel) 14 (11) (2021) http://dx.doi.org/10.3390/ma14112991.

[37] Z. Li, P. Liu, Y. Yuan, X. Liang, J. Lei, X. Zhu, et al., Loss of longitudinal superiority marks the microarchitecture deterioration of osteoporotic cancellous bones, Biomech. Model. Mechanobiol. 20 (5) (2021) 2013–2030, http://dx.doi.org/10.1007/s10237-021-01491-z.

[38] P. Liu, X. Liang, Z. Li, X. Zhu, Z. Zhang, L. Cai, Decoupled effects of bone mass, microarchitecture and tissue property on the mechanical deterioration of osteoporotic bones, Composites B 177 (2019) 107436, http://dx.doi.org/10.1016/j.compositesb.2019.107436.

[39] R. Rafiee-Dehkharghani, A.J. Aref, G.F. Dargush, Planar stress wave attenuation in plates with circular voids and inclusions, Composites B 75 (2015) 307–318, http://dx.doi.org/10.1016/j.compositesb.2015.01.051.